Auger Electron Spectra

The Basic Data for Understanding the Auger Effect

Ekkehard Pomplun

From Abteilung Sicherheit und Strahlenschutz, Forschungszentrum Jülich GmbH, Jülich, Germany

Correspondence to: Ekkehard Pomplun, Abteilung Sicherheit und Strahlenschutz, Forschungszentrum Jülich, 52425 Jülich, Germany. Fax: + 49 2461 613726. E-mail: e.pomplun@fz-juelich.de

Acta Oncologica Vol. 39, No. 6, pp. 673–679, 2000

Understanding the strong radiotoxicity of DNA-incorporated Auger electron-emitting nuclides requires a detailed knowledge of the nuclide's emission spectrum. A Monte Carlo computer code was previously developed to simulate Auger cascades and to provide electron spectra of ^{125}I. To utilize experimental data for a direct validation of these simulations, the code has been adapted for cascades in xenon, which is adjacent to iodine in the table of elements. Only minor modifications of the code were necessary to obtain a very good agreement with the experimental findings. The role of shake-off electrons and the need for energy considerations during the cascades could be demonstrated. A previously published electron spectrum of ^{125}I was recalculated and detailed results are presented here. Furthermore, to consider implications from a molecular binding of the Auger emitter, for the first time semi-empirical quantum mechanical calculations for an iodine-labelled thymine molecule were performed showing that even in the condensed phase a Coulomb explosion cannot be excluded a priori.

Received 22 September 1999
Accepted 4 April 2000

Since the first experimental findings of severe chromatin damage by DNA-incorporated ^{125}I (1, 2), different mechanisms have been discussed to explain this so-called 'Auger effect': the shower of low-energy Auger electrons released during the decay of ^{125}I, the transmutation of iodine to tellurium and the chemical alterations involved, the recoil of the decaying nucleus, and, last but not least, a 'Coulomb explosion' according to fragment ion distributions found after the decay of molecular-bound ^{125}I in the gaseous phase (3, 4). The recoil energy has been evaluated as being too small for inducing an effect like the Auger one. Also, the iodine and its chemistry can be excluded because the strongly biologically damaging efficiency of ^{125}I has been determined (1) in contrast to another iodine isotope, ^{131}I, which undergoes β^- decay. Whereas ^{125}I decays to tellurium, ^{131}I goes to xenon, so theoretically the transmutation to tellurium could be the responsible reason; however, a significant difference in the biological effectiveness was also demonstrated between the two iodine isotopes ^{125}I and ^{123}I (5), both decaying to tellurium.

Therefore, to understand the strong radiotoxicity of DNA-bound Auger emitters the physical processes involved in the reorganization of the electron cloud after inducing an inner shell vacancy have to be considered. These processes determine the emission of Auger electrons and the build-up of charges. The inner shell vacancy is created by the initial decay event, i.e. by electron capture or internal conversion. The excess energy is released by a series of subsequent transitions that can be assumed to proceed like a cascade (6) in about 10^{-16}–10^{-14} s. The most important transitions are the Auger and Coster–Kronig transitions, which emit an electron and thereby increase the charge on the atom, and also radiative transitions, which emit an x-ray. Moreover, a number of further mechanisms have been observed, for example shake-off, shake-up, double Auger emission, etc. (7, 8). According to the stochastic character of all of these transitions, a huge number of pathways exist by means of which the excited atom can de-excite, i.e. each initial inner shell hole may cause a different number of Auger electrons to be emitted resulting in a more or less broad distribution of differently charged ions.

Because these electron transitions are random processes, the Monte Carlo (MC) technique is an appropriate tool for the simulation of Auger cascades and electron spectra. Up to now, several authors have developed MC-based computer codes either to simulate photon-induced cascades in noble gases (6, 9–11) for the interpretation of experimentally found charge distributions, or to investigate cascades in nuclides like ^{125}I, which are of special interest in radiobiology or nuclear medicine (e.g. (12–18)). Al-

 ISSN 0284-186X

though nearly all of these codes refer to the same databases for cross-sections, transition probabilities, etc. (see 'Methods'), there are a number of significant differences. Some investigators of the radiobiological relevant nuclides have assumed an extremely fast charge transfer by electrons from the molecular environment ('condensed phase'), enabling an immediate neutralization of vacancies in the valence shells and thereby prohibiting charge accumulation and subsequent Coulomb explosion. Since a charge transfer in less than 10^{-14} s is difficult to understand physically (13), other authors (12, 17) have not allowed neutralization during the cascades ('isolated atom'). Owing to this open question, also for the condensed phase, an accumulation of charges in the valence shells is still under debate.

Another difference is due to the methods used to determine the kinetic electron energies. For the noble gas investigations (6, 9–11) the differences among the binding energies of neutral atoms have been used. A more accurate method, the modified $(Z+1)$ approximation, has been introduced for the first simulation of ^{125}I cascades (13) and applied for several other nuclides (14–16, 18). However, neither method can fully take into account the shift of electron energy levels owing to the multiple ionizations during the cascade. Therefore, a different method has been developed that is based on the total energy of the individual atomic states before and after a transition (see 'Methods' and (12)). Furthermore, shake-off electrons seem to be of minor influence for cascades owing to their relatively low probabilities (7) so that they are not considered by all codes.

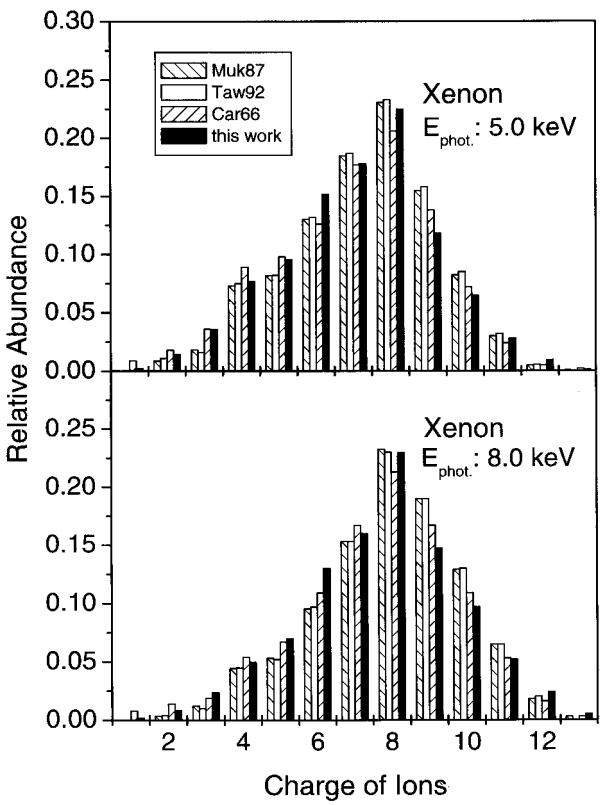

Fig. 1. Charge distribution after photoionization in xenon: comparison with experimental results from synchrotron [Muk87 (11), Taw92 (20)] and x-ray [Car66 (19)] irradiation of 5 and 8 keV.

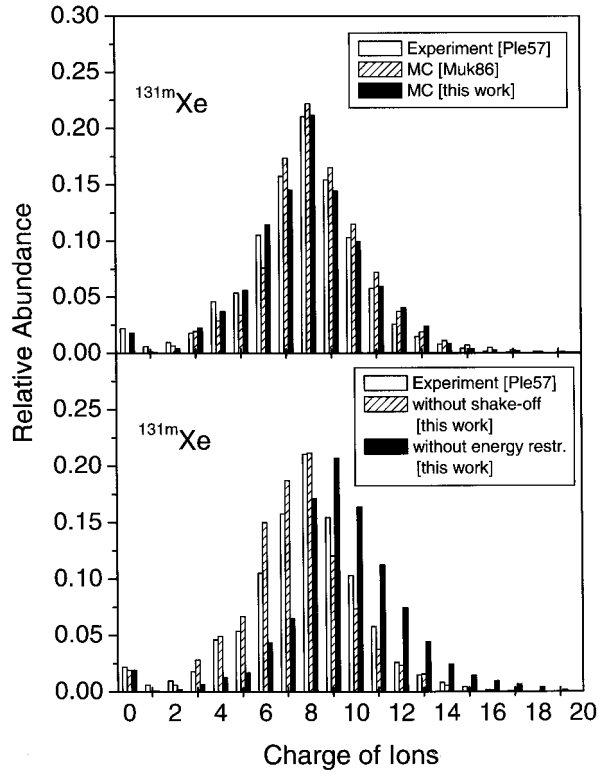

Fig. 2. Charge distribution after de-excitation of ^{131m}Xe. (a) Comparison with experiment [Ple57 (21)] and MC simulations [Muk86 (10)]; (b) comparison between experiment [Ple57 (21)] and modified MC simulations neglecting shake-off and energy restrictions (this work).

Table 1

Mean number of charges after decay of ^{131m}Xe

References	Incl. Neutrals	Excl. neutrals
Experiment (21)	7.73 ± 0.05	7.91 ± 0.05
MC (this work)	7.81	7.96
MC (10)	–	8.37

A major disadvantage connected with the MC results for the radioisotopes is the lack of experimental data, so a direct comparison has not been possible until now. Therefore, and owing to the problems discussed above, the intentions of this paper are as follows: (a) to validate the methods and assumptions of the MC code used in (12) by adapting it for the simulation of photoionization experiments with xenon (11, 19, 20), adjacent to iodine in the table of elements, and of ^{131m}Xe de-excitation measurements (21). In particular, the significance of energy determination during the cascades and of the inclusion of

shake-off electrons will be investigated. (b) To provide an improved and more detailed spectrum of ^{125}I for both the 'isolated atom' and the 'condensed phase' case on the basis of the validated MC code. (c) To elucidate the possibility of 'Coulomb explosion' in the condensed phase by performing semi-empirical quantum mechanics calculations on the stability of an iodine-labelled thymine molecule as a function of increasing charge.

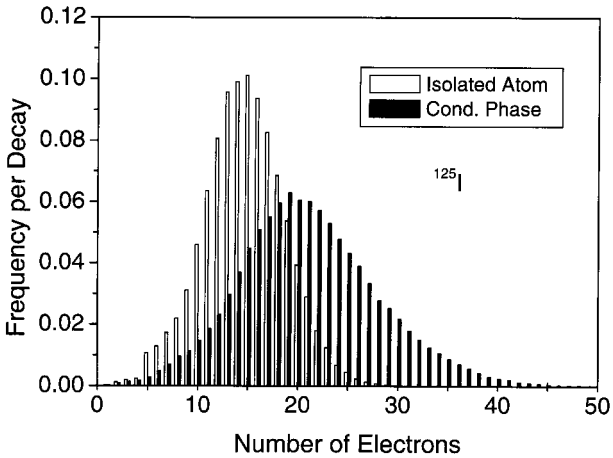

Fig. 3. Frequency distribution of the number of emitted electrons for 'isolated atom' and 'condensed phase'.

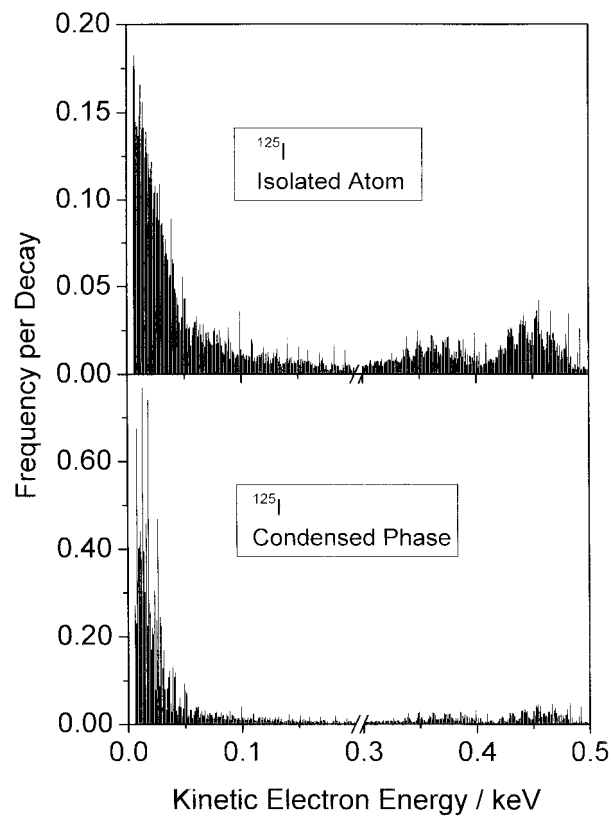

Fig. 4. Electron spectrum up to 0.5 keV after decay of ^{125}I for 'isolated atom' and 'condensed phase'.

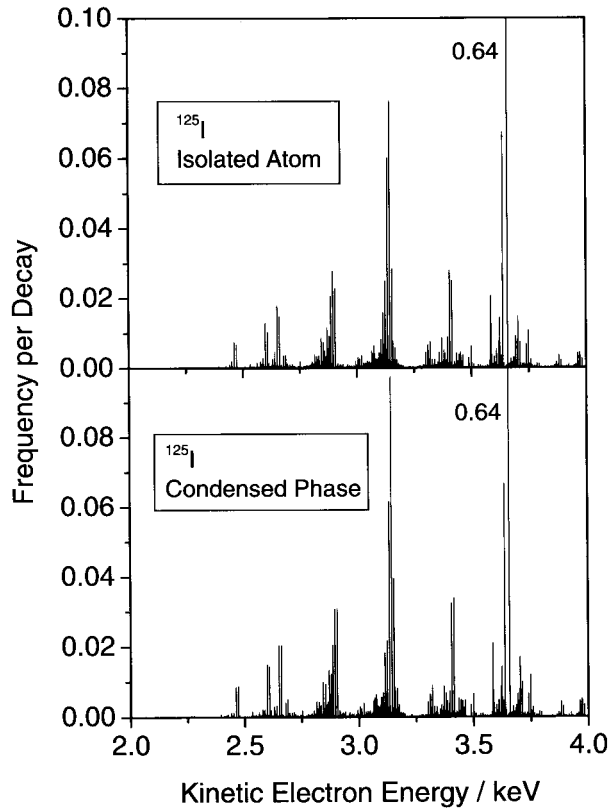

Fig. 5. Electron spectrum in the range between 2.0 and 4.0 keV after decay of ^{125}I for 'isolated atom' and 'condensed phase'.

METHODS

A detailed description of the simulation code used here has been given elsewhere (12); in the following, only the main aspects will be briefly summarized. In the first step, the MC program selects the sub-shell, which will be ionized according to photoionization cross-sections (22, 23) or to capture and internal conversion probabilities (for references see (13)). Next, the transition to the initial hole is picked out randomly from a list of possible radiative (photon) and non-radiative (Auger and Coster–Kronig) processes. For the photon transitions, relative intensities to K- and L-shells (24) have been normalized to fluorescence yields (25); probabilities of Auger and Coster–Kronig transitions to K- and L-shells were taken from (26), to higher shells from (27, 28) and of shake-off processes from (7). All these transition probabilities are for singly ionized atoms, although they were modified according to the actual number of electrons available in the shells involved in the selected transition. After recording the new electron configuration, the total energy of this individual atomic state is calculated by a code based on the relativistic Dirac–Fock method (29). The difference of the energy

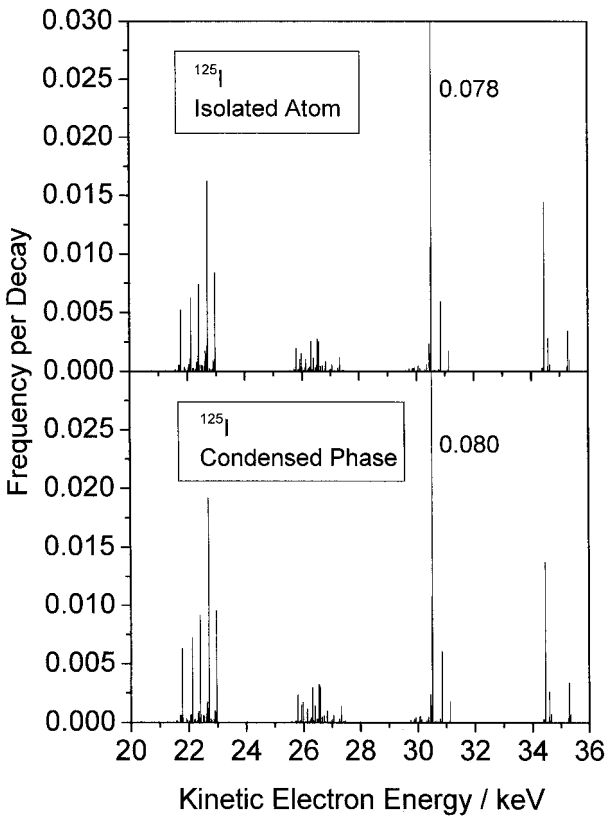

Fig. 6. Electron spectrum in the range between 20 and 36 keV after decay of ^{125}I for 'isolated atom' and 'condensed phase'.

values between the initial (before the transition) and the final electron configuration (after the transition) is equal to the kinetic energy of the emitted electron or x-ray. Furthermore, this procedure allows transitions that are not energetically possible to be rejected. Finally, it is chosen to fill the hole situated at the lowest level in the next transition. Other transition sequences have also been tried, for example filling the highest vacancy first, or filling holes according to the width of the states. However, these modifications yielded poor charge distributions compared with experimental results (data not shown here). For each simulated experiment 100000 MC runs, i.e. either photo-effects or decays, were performed.

The semi-empirical quantum mechanics calculations were performed by applying the PM3 method (30, 31) within the HyperChem™ program system (32). In this calculation model, the methyl group of thymine was replaced by iodine and then by tellurium. Subsequently, the charge on the molecule was increased in steps of one unit.

Table 3

Bond length between the decaying iodine and the C5 atom of the thymine molecule as a function of charge

Bond	Total charge	Bond length [Å]
CH_3–C5	0	1.50
I–C5	0	1.96
Te–C5	0	2.07
Te–C5	+1	1.98
Te–C5	+2	1.90
Te–C5	+3	2.11
Te–C5	+4	2.23
Te–C5	+5	2.67
Te–C5	+6	(4.68)

Table 2

Transition yields and mean Auger (AUG), Coster–Kronig (CK) and conversion (CE) electron energies for ^{125}I

Transition	Yield/decay (isolated atom)	Yield/decay (cond. phase)	Mean energy [keV] (isolated atom)	Mean energy [keV] (cond.phase)
CE–K	8.03E−01	8.03E−01	3.64E+00	3.64E+00
CE–L_1	9.47E−02	9.69E−02	3.05E+01	3.05E+01
CE–L_2	7.22E−03	7.61E−03	3.09E+01	3.09E+01
CE–L_3	2.02E−03	1.93E−03	3.11E+01	3.11E+01
CE–M_1	1.71E−02	1.65E−02	3.45E+01	3.45E+01
CE–M_2	3.34E−03	3.21E−03	3.46E+01	3.46E+01
CE–M_3	8.80E−04	8.80E−04	3.47E+01	3.47E+01
CE–N_1	3.91E−03	3.90E−03	3.53E+01	3.53E+01
CE–N_2	1.13E−03	8.10E−04	3.53E+01	3.53E+01
AUG–KLL	1.32E−01	1.33E−01	2.25E+01	2.25E+01
AUG–KLX	5.78E−02	5.80E−02	2.64E+01	2.64E+01
AUG–KXY	5.15E−03	5.48E−03	3.02E+01	3.02E+01
CK–LLX	2.64E−01	2.67E−01	2.81E−01	2.85E−01
AUG–LMM	1.24E+00	1.25E+00	3.03E+00	3.04E+00
AUG–LMX	3.46E−01	3.44E−01	3.66E+00	3.67E+00
AUG–LXY	2.24E−02	2.21E−02	4.30E+00	4.29E+00
CK–MMX	1.48E+00	1.49E+00	9.14E−02	9.42E−02
AUG–MXY	3.30E+00	3.31E+00	4.00E−01	4.05E−01
CK–NNX	3.21E+00	3.33E+00	2.93E−02	3.16E−02
AUG–NXY	2.15E+00	8.12E+00	2.07E−02	1.61E−02

RESULTS AND DISCUSSION

Xenon

MC calculations were performed to simulate three different experiments: photoionization by synchrotron radiation (11, 20) and x-rays (19) with energies of 5.0 and 8.0 keV, which are above the L_3- and the L_1-shell, respectively, and the isomeric transition of ^{131m}Xe (21), which leads predominantly to K-shell ionization (61%) owing to internal conversion. Whereas the synchrotron radiation results (11, 20) are nearly identical for both energies, the x-ray data (19) deviate slightly towards smaller charges because of their non-monochromatic photons. This shift is expressed in the mean charge values of 7.3 (11) versus 6.95 (19) for the 5.0 keV photons and 7.97 (11) versus 7.59 (19) for 8.0 keV. The MC ion distributions found in this work (Fig. 1) agree very well with the experimental results. The breadth and the positions of the maximum (Xe^{8+}) are the same for both photon energies. Compared with (11) and (20), the poorest agreement is for Xe^{6+} (2.0% and 3.3% differences for 5.0 keV and 8.0 keV, respectively) and for Xe^{9+} (4.0% and 4.3%). Although the MC results are obtained by also assuming monochromatic incident photons, the agreement with the x-ray data (19) is even better than with the synchrotron data (11, 20). The greatest differences from (19) are at Xe^{6+} (2.5% in the 5.0 keV and 2.1% in the 8.0 keV experiment) and at Xe^{9+} (2.0% for both energies). A slight overestimation of all those charge values smaller than the maximum (8 +) corresponds to an underestimation of higher charges.

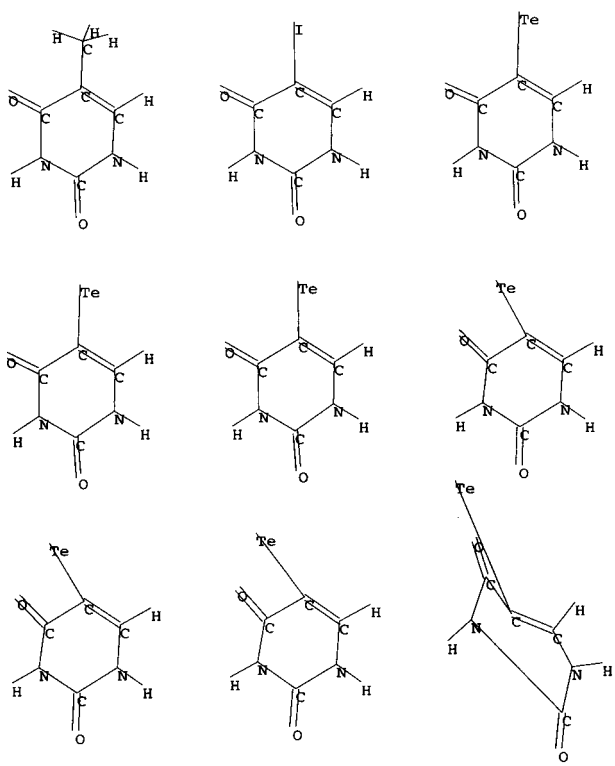

Fig. 7. Stick model of the DNA base thymine (top row, left) after geometry optimization, with iodine replacing the methyl group (top, centre) and tellurium replacing the iodine (top, right); the next six graphs give the results after increasing the charge on the model from + 1 (centre row, left) up to + 6 (bottom row, right).

The charge distribution found for the isomeric transition of ^{131m}Xe follows the experimental data (21) very smoothly with only small deviations (see Fig. 2a), the greatest of which is 1.5% at Xe^{12+}. For a comparison with another MC simulation (10) see Fig. 2a, and for mean charge values see Table 1. The differences in the two theoretical distributions (10, this work) can be partially attributed to the different initial vacancy distributions applied. A fraction of 2.2% (21) and 1.9% (33) is reported for γ-emission (instead of inner shell hole induction), which does not produce any charge; these values have also been used in this work whereas in (10) γ-emission is completely neglected (34). The mean charge values in column 3 of Table 1 have been corrected for these neutrals. The remaining differences between this work and (10) are assumed to be due to different energy calculation approaches. However, this point must remain uncertain because no details are given in (10).

It should be noted that the charge distribution after ^{131m}Xe de-excitation is similar to that following photoionization of the L-shell, in particular in the region around the maximum value (Xe^{8+}). The reason is to be found in the high relative probability for radiative transition to the K-shell (0.893 (26)), transferring initial K-holes to L- or higher shells without increasing the charge. The better agreement with the ^{131m}Xe experiments than with the photoionization of L-shells seems to indicate that the differences in Fig. 1 are not because of the cascades but because of inaccurate initial vacancy distributions.

The need for a strict energy consideration as well as the influence of shake-off electrons for the cascades is demonstrated in Fig. 2b. Here, the experimental results are compared with two modified MC simulation modes. In the first one, no energies were calculated so that any transition from the given list was allowed as long as the levels involved were not fully depleted. The second one did not consider shake-off processes. It can be seen that testing the energetic conditions for the individual transition is essential, otherwise quite a different charge distribution is obtained with a mean value of + 9.4 (values determined experimentally are between + 7.7 and + 7.9; see Table 1), and there are consequently significant differences in the number of emitted electrons. The influence of the shake-off electrons on the shape of the charge distribution is evident from a comparison of Fig. 2a and 2b. The agreement with the experiments (Fig. 2a) becomes poorer with differences of 4.5% (+ 6), 3.0% (+ 7), 3.4 (+ 9), and 3.0% (+ 10). Although these electrons amount to less than 10% of all electrons released during ^{131m}Xe isomeric transition (0.67 shake-off electrons per de-excitation), they obviously play

a very sensitive role with regard to the stochastic pathway the de-excitation process takes from the inner shell vacancy until all charges have been shifted to the valence shells.

Iodine-125

The good agreement of the xenon data reported here with the experimental distribution seems to indicate that the cascade itself, i.e. the transitions, their energies and their probabilities, is reasonable and, moreover, that all significant processes have been considered. However, for a molecular bound isotope such as ^{125}I in the form of ^{125}I-IUdR, the situation is much more complex than for a noble gas. As has been discussed in the introduction, the question of possible charge transfer to neutralize vacancies very strongly influences the number of emitted electrons (12, 13). In the simulation, all vacancies will be neutralized during the metastable ^{125}Te state (1.6×10^{-9} s) to which ^{125}I decays by electron capture before going to the ^{125}Te ground state via internal conversion. Moreover, the condensed phase condition in Figs. 3–6 means an immediate neutralization of valence shell vacancies also during the cascades, whereas in the isolated atom case these fast charge transfers are not allowed.

To illustrate the influence of a fast neutralization on the number of emitted electrons, both approaches have been considered here resulting in a difference of six electrons emitted per decay (15 and 21 in cases of isolated atom and condensed phase, respectively; see Fig. 3). Table 2 gives the probabilities and mean energies for individual transitions and conversion electrons.

Based on the assumptions and the same data sources applied for the xenon cascades, the electron spectrum for ^{125}I was also simulated here and the results are displayed for three different energy ranges in Fig. 4, Fig. 5 and Fig. 6, with a bin width of 1 eV. Whereas for the kinetic energies above 2 keV only minor differences can be seen between isolated atom and condensed phase conditions, there are large discrepancies at energies below 50 eV (see Fig. 4; note the different scaling of the ordinates). This is the region of Coster–Kronig–NNX and Auger–NXY transitions (see Table 2), which are strongly dependent on the electron population of the valence shells, which, vice versa, depends on the possibility of re-filling depleted shells immediately by a very fast charge transfer.

Iodine-labelled thymine

The results of the semi-empirical quantum mechanical calculations for the ^{125}I-IUdR molecule are characterized here by the bond lengths between the iodine/tellurium atom and the C5 atom (Table 3) and by the structure of the stick models after geometry optimization and single-point energy calculation (Fig. 7). The consequences of an increasing charge in the valence shells can be seen very clearly. As long as the charge is below $+5$ there are only small alterations. At $+5$, the bond length increases by more than 20% compared with the $+4$ state. At $+6$ the calculations no longer converge and a stable structure does not seem to be possible. This could also mean that in case the of ^{125}I, the second cascade induced by the internal conversion after the decay of the metastable state would take place when the atom is perhaps no longer part of the molecule and may have been moved away from the original position. It is obvious that these data need further confirmation, for example by 'ab initio' calculations; however, they demonstrate that a Coulomb explosion or at least a severe structural deformation of the molecule cannot be excluded a priori. If these mechanisms contribute to the biological effect, the classical relative biological effectiveness concept would not be appropriate for molecular-bound Auger electron emitters.

ACKNOWLEDGEMENTS

This work was supported in part by the German Federal Environment Ministry (StSch 4124).

REFERENCES

1. Hofer KG, Hughes WL. Radiotoxicity of intranuclear tritium, ^{125}Iodine and ^{131}Iodine. Radiat Res 1971; 47: 94–109.
2. Feinendegen LE, Ertl HH, Bond VP. Biological toxicity associated with the Auger effect. In: Ebert H, ed. Proceedings of the Symposium on Biophysical Aspects of Radiation Quality. Vienna: IAEA, 1971: 419–30.
3. Carlson TA, White RM. Measurement of the relative abundances and recoil-energy spectra of fragment ions produced as the initial consequences of x-ray interaction with CH_3I, HI, and DI. J Chem Phys 1966; 44: 4510–20.
4. Carlson TA, White RM. Formation of fragment ions from CH_3Te^{125} and $C_2H_5Te^{125}$ following the nuclear decays of CH_3I^{125} and $C_2H_5I^{125}$. J Chem Phys 1963; 38: 2930–4.
5. Makrigiorgos M, Kassis AI, Baranowska-Kortylewicz J, et al. Radiotoxicity of 5-[^{123}I]Iodo-2′-deoxyuridine in V79 Cells: a comparison with 5-[^{125}I]Iodo-2′-deoxyuridine. Radiat Res 1989; 118: 532–44.
6. Krause MO, Carlson TA. Vacancy cascade in the reorganization of krypton ionized in an inner shell. Phys Rev 1967; 158: 18–24.
7. Carlson TA, Nestor CW. Calculation of electron shake-off probabilities as the result of x-ray photoionization of the rare gases. Phys Rev 1973; A8: 2887–94.
8. Carlson TA, Krause MO. Experimental evidence for double electron emission in an Auger process. Phys Rev Lett 1965; 14: 390–2.
9. Carlson TA, Krause MO. Atomic readjustment to vacancies in the K and L shells of argon. Phys Rev 1965; 137: 1655–62.
10. Mukoyama T. Monte Carlo simulations of vacancy cascade in Xe. J Phys Soc Jpn 1986; 55: 3054–8.
11. Mukoyama T, Tonuma T, Yagishita A, et al. Charge distribution of Xe ions as a result of multiple photoionisation of Xe atoms between 4.1 and 8.0 keV. J Phys B: At Mol Phys 1987; 20: 4453–60.
12. Pomplun E, Booz J, Charlton DE. A Monte Carlo simulation of Auger cascades. Radiat Res 1987; 111: 533–52.
13. Charlton DE, Booz J. A Monte Carlo treatment of the decay of ^{125}I. Radiat Res 1981; 87: 10–23.

14. Rao DV, Govelitz GF, Sastry KSR. Radiotoxicity of thallium-201 in mouse testes: inadequacy of conventional dosimetry. J Nucl Med 1983; 24: 145–53.
15. Humm JL. The analysis of Auger electrons released following the decay of radioisotopes and photoelectric interactions and their contribution to energy deposition. Berichte der Kernforschungsanlage Jülich, Jül–1932, 1984, ISSN 0366–0885.
16. Sastry KSR, Rao DV. Dosimetry of low energy electrons. In: Rao DV, Chandra R, Graham MC, eds. Physics of nuclear medicine. Recent advances. New York: American Institute of Physics, 1984: 169–208.
17. Pomplun E. ^{123}I: Calculation of the Auger electron spectrum and assessment of the strand breakage efficiency. In: Howell RW, Narra VR, Sastry KSR, Rao DV, eds. Biophysical aspects of Auger processes. Woodbury, NY: American Institute of Physics, 1992: 121–36.
18. Howell RW. Radiation spectra for Auger-electron emitting radionuclides. Report No. 2 of AAPM Nuclear Medicine Task Group No.6. Med Phys 1992; 19: 1371–83.
19. Carlson TA, Hunt WE, Krause MO. Relative abundances of ions formed as the result of inner-shell vacancies in atoms. Phys Rev 1966; 151: 41–7.
20. Tawara H, Hayaishi T, Koizumi T, et al. Production of multiply charged Xe^{i+} ions via photoionization and excitation in the L-edge region. J Phys B: At Mol Opt Phys 1992; 25: 1467–73.
21. Pleasonton F, Snell AH. Ionization following internal conversion in xenon. Proc Roy Soc London 1957; 241A: 141–52.
22. Scofield JH. Theoretical photoionization cross sections from 1 to 1500 keV. Report UCRL-51326. US Atomic Energy Commission, 1973.
23. Band IM, Kharitonov YI, Trzhaskovskaya MB. Photoionization cross sections and photoelectron angular distributions for X-ray line energies in the range 0.132–4.509 keV; Targets: $1 \leq Z \leq 100$. At Data Nucl Data Tables 1979; 23: 443–505.
24. Storm E, Israel HI. Photon cross sections from 1 keV to 100 MeV for elements $Z = 1$ to $Z = 100$. Nucl Data Tables 1970; A7: 565–681.
25. Krause MO. Atomic radiative and radiationless yields for K and L shells. J Phys Chem Rev Data 1979; 8: 307–27.
26. Chen MH, Crasemann B, Mark H. Relativistic radiationless transition probabilities for atomic K- and L-shells. At Data Nucl Data Tables 1979; 24: 13–37.
27. McGuire EJ. M-shell Auger and Coster–Kronig electron spectra. Phys Rev 1972; A5: 1052–9.
28. McGuire EJ. Atomic N-shell Coster–Kronig, Auger, and radiative rates and fluorescence yields for $38 \leq Z \leq 103$. Phys Rev 1974; A9: 1840–51.
29. Desclaux JP. A multiconfiguration relativistic Dirac–Fock program. Comput Phys Commun 1975; 9: 31–45.
30. Stewart JJP. Optimization of parameters for semiempirical methods. I. Method. J Comput Chem 1989; 10: 209–20.
31. Stewart JJP. Optimization of parameters for semiempirical methods. II. Applications. J Comput Chem 1989; 10: 221–64.
32. HyperChem™. Computational chemistry, molecular visualization and simulation. Publication HC40-00-03-00. Waterloo, Ontario: Hypercube, Inc., April 1994.
33. ICRP 1983 Radionuclide Transformations. Publication 38, International Commission on Radiological Protection. Oxford: Pergamon Press.
34. Wolfson JL, Park JJH, Yaffe L. Internal conversion spectrum of I^{131} (8.06 d). Nuc Phys 1962; 39: 613–20.